8.5 A 6nA Fully-Autonomous Triple-Input Hybrid-Inductor-Capacitor Multi-Output Power Management System with Multi-Rail Energy Sharing, All-Rail Cold Startup, and Adaptive Conversion Control for mm-scale Distributed Systems

Xinjian Liu, Anjali Agrawal, Akiyoshi Tanaka, Benton Calhoun

University of Virginia, Charlottesville, VA

2024 IEEE International Solid-State Circuits Conference (ISSCC) | 979-8-3503-0620-0/24/$31.00 ©2024 IEEE | DOI: 10.1109/ISSCC49657.2024.10454435

Advancements in power and size reduction for integrated circuits (IC) enable integration of self-powered systems into mm-scale fiber strand [1]. Moving towards intricate fiber networks where multiple subsystems interact within textiles, energy harvesting and power management units (EHPMU) require full autonomy, ultra-low quiescent power, high efficiency, and mm-scale footprint. Additionally, they must coordinate energy across distributed subsystems for enhanced viability and scalability. A switched-capacitor (SC) based EHPMU [1] realizes distributed energy sharing but has constrained efficiency and dynamic range (<5μW). Also, its single-rail-sharing architecture forces all subsystems to interact with a shared rail, necessitating extra dedicated converters. Existing multi-input single-inductor multi-output (MISIMO) EHPMUs [2–7] either consume >100nW quiescent power [3–7], have <1000× dynamic range [3][5], lack full autonomy [3, 4, 6, 7], or require large inductor (22μH) with low efficiency due to conventional buck-boost (CBB) conversion [2]. Furthermore, none of them support distributed systems. As shown in Fig. 8.5.1, we address these limitations with a fully autonomous triple-input hybrid-inductor-capacitor multi-output (TIHICMO) EHPMU that can harvest energy from dual input sources, regulate three custom output rails, adaptively switch among multi-conversion methods, cold startup (CS) from all the inputs/outputs, and enable energy recycling and sharing among multiple rails. This EHPMU achieves a 5.8nA quiescent current, a wide dynamic range of $8.8\text{x}10^4$, a peak efficiency of 90.1%, and a >90% reduction in inductor size compared to [2, 7] using a 3×3×1.3mm³ 200mΩ DCR inductor.

To meet these demands, the proposed EHPMU improves the traditional architectures by: 1) multi-rail energy sharing: this EHPMU extracts energy from a photovoltaic (PV) cell and a thermoelectric generator (TEG) cell while generating three regulated output rails: V_{DIG} (0.55 to 0.65V), V_{ANA} (1 to 1.1V) and V_{IO} (1.6 to 1.7V) with one power-delivery stage. It automatically transitions among four operating modes: harvest (V_{INs} to V_{OUTs}), store (V_{INs} to V_{STO}), backup (V_{STO} to V_{OUTs}), and a proposed recycle mode (V_{OUTs} to V_{STO}), as shown in Fig. 8.5.1. In a distributed network with subsystems having their local energy harvesters, the recycle mode empowers the EHPMU to recycle and redistribute the surplus energy from energy-abundant subsystems to the energy-scarce ones. This fosters energy sharing across different voltage domains and the expansion towards more comprehensive networks; 2) all-rail cold startup (AR-CS): the EHPMU can cold startup from any input and output rail. Subsystems can trigger the EHPMU's startup, allowing the surplus energy to be reallocated promptly. Thus, subsystems can collectively launch and maintain the fiber network, reducing environmental reliance. 3) TIHICMO architecture: the two off-chip 0.4×0.2mm² flying capacitors (C_{FLY}) enables a hybrid-inductor-capacitor (HIC) conversion method by serially connecting the inductor and C_{FLY} to reduce the inductor voltage, enabling inductor size reduction without sacrificing efficiency. In addition, a dual-step conversion is proposed for high voltage conversion ratio. The V_{ANA} rail serves as an intermediate level, allowing the energy to be harvested and then recycled, achieving higher overall efficiency. Based on the input and output voltage levels, this EHPMU dynamically adapts its conversion methods among CBB conversion [2, 6, 7], buck/boost-based conversion [3, 4], HIC conversion and dual-step conversion, ensuring high efficiency across a wide input/output range.

The left of Fig. 8.5.2. shows the system block diagram of the proposed EHPMU. To minimize the quiescent current and maximize efficiency, several techniques are used: 1) Instead of uniformly driving power-stage switches (PSS) with the highest voltage (V_{MAX}) [2], a portion of the PSS is driven by the V_{IO} rail, reducing the switching loss by >70%; 2) each input and output rail has its own comparator, clock, and pulse-frequency-modulation. The Mode&Gate Control (MGC) incorporates an asynchronous timing generator (ATG), activated only by events from input/output rails, further reducing dynamic power; 3) with negligible dynamic loss, we further suppress the quiescent current without efficiency degradation by a customized 500nm length I/O device standard-cell library, compared with core devices [2]; 4) The EHPMU adopts an ADC-based current-discharging mechanism for constant peak inductor current (I_{PEAK}) control, eliminating the need for power-intensive comparators, as seen in traditional adaptive-on-time (AOT) controller [3, 4]. The right of Fig. 8.5.2. shows the schematic of the C_{FLY} pre-charger and the algorithm for source and load selection, outlined as follows: when the MGC is triggered, it checks load and source events with a priority: REQ>FULL>MPP. For each event, the MGC follows the load/source rail priority (V_{IO}>V_{ANA}>V_{DIG}, V_{PV}>V_{TEG}>V_{STO}) to check the corresponding signal for each rail. Power delivery is initiated when both the source and load are identified.

Figure 8.5.3. shows the circuit details of the proposed AR-CS, AOT, and adaptive off-time (AOFT) control along with the timing waveforms. The AR-CS consists of four stages, with each of the initial three stages featuring a clock, a voltage monitor (VM) or power-on-reset, and a SC-based converter. The VM regulates the V_{DIG} and V_{ANA} rails to ranges of 0.6 to 0.7V and 0.9 to 1V, respectively. Initially, all the output rails are shorted via M_{1-3} and charged concurrently. When the input voltages of the 2nd/3rd stage exceed the threshold, the converter is activated and the connection to the subsequent stage is disabled via the DIS_D/DIS_A signals, allowing the next stage to be charged to a higher voltage level. Once the V_{IO} rail reaches 1.5V, maximal-power-point tracking (MPPT) and ADC sampling are enabled. Subsequently, POR_{SYS} triggers the main EHPMU and power-gates the AR-CS. The AOT and AOFT control use a tunable bias current to discharge a capacitor for I_{PEAK} control, as shown in the bottom of Fig. 8.5.3. Given that the V_{PV}/V_{TEG}/V_{STO} rails are digitized by the ADC, the on/off-time calculator adjusts the bias current to maintain proportionality to the inductor voltage, ensuring constant I_{PEAK}.

The proposed TIHICMO EHPMU is fabricated in 65nm CMOS. The testbench for CS is shown in Fig. 8.5.4. The measured waveform shows that the EHPMU successfully cold startup from the V_{TEG} rail, followed by the regulation of output rails and simultaneous harvesting from V_{PV} and V_{TEG} rails using fractional open-circuit voltage (FOCV) based MPPT. The measured waveform also shows the EHPMU's ability to CS from an output rail. The subsystem can harvest energy from its local PV cell to charge the V_{ANA} rail, triggering the startup of the EHPMU. Then the EHPMU actively recycles the surplus energy and redistributes it. The EHPMU's ability of concurrently regulating all rails and switching among different operating modes is also validated, with a zoomed-in part showing the transition from harvest mode to backup mode and the initiation of C_{FLY} pre-charging. The measured quiescent power in Fig. 8.5.5. shows a minimum quiescent current of 5.8nA at 1.6V. The proposed dual-step conversion improves the efficiency by 10% at high voltage conversion ratio. Measurements also show that the EHPMU achieves a >25% efficiency improvement compared to CBB conversion, a 4-to-7% efficiency improvement compared to the buck-based conversion, a peak efficiency of 90.1%, and an efficiency >50% over an 8,8000× dynamic range.

Figure 8.5.6. presents a comparison with the state-of-the-art MISIMO EHPMUs. Among the state-of-the-art designs shown in table in Fig. 8.5.6, the proposed EHPMU achieves the lowest quiescent power with the widest dynamic range. Thanks to the HIC architecture, this EHPMU achieves a >90% inductor size reduction compared to [2, 6] with a competitive 90.1% peak efficiency and a highest efficiency when delivering 1μA output current with a 200mΩ DCR inductor. Moreover, with the proposed AR-CS technique and recycle mode, this EHPMU can cold startup from any input and output rail, and achieve energy sharing across voltage domains, a capability absents in previous works. All these results and features make this EHPMU well-suited for mm-scale, self-powered, and distributed systems. Figure 8.5.7. shows a micrograph of the EHPMU with a 1.4×2.0mm² die area.

Acknowledgement:
This material is based upon work supported by the Under Secretary of Defense for Research and Engineering under Air Force Contract No. FA8702-15-D-0001. Any opinions, findings, conclusions, or recommendations expressed in this material are those of the authors and do not necessarily reflect the views of the Under Secretary of Defense for Research and Engineering.

References:
[1] X. Liu et al., "A Self-Powered SoC with Distributed Cooperative Energy Harvesting and Multi-Chip Power Management for System-in-Fiber," *ISSCC*, pp. 236–237, Feb. 2023.
[2] S. Li et al., "A 32nA Fully Autonomous Multi-Input Single-Inductor Multi-Output Energy-Harvesting and Power-Management Platform with $1.2\text{×}10^5$ Dynamic Range, Integrated MPPT, and Multi-Modal Cold Start-Up," *ISSCC*, pp. 472–473, Feb. 2022.
[3] C.-W. Liu et al., "Dual-Source Energy-Harvesting Interface with Cycle-by-Cycle Source Tracking and Adaptive Peak-Inductor-Current Control," *IEEE JSSC*, vol. 53, no. 10, pp. 2741–2750, Oct. 2018.
[4] H. Kim et al., "A 90.2% Peak Efficiency Multi-Input Single-Inductor Multi-Output Energy Harvesting Interface with Double-Conversion Rejection Technique and Buck-Based Dual-Conversion Mode," *IEEE JSSC*, vol. 56, no. 3, pp. 961–971, Mar. 2021.
[5] P.-H. Chen et al., "A Single-Inductor Triple-Source Quad-Mode Energy-Harvesting Interface with Automatic Source Selection and Reversely Polarized Energy Recycling," *IEEE JSSC*, vol. 54, no. 10, pp. 2671–2679, Oct. 2019.
[6] S.S. Amin et al., "MISIMO: A Multi-Input Single-Inductor Multi-Output Energy Harvester Employing Event-Driven MPPT Control to Achieve 89% Peak Efficiency and a 60,000x Dynamic Range in 28nm FDSOI," *ISSCC*, pp. 144-146, Feb. 2018.
[7] G. Yu et al., "A 400 nW Single-Inductor Dual-Input-Tri-Output DC-DC Buck-Boost Converter With Maximum Power Point Tracking for Indoor Photovoltaic Energy Harvesting," *IEEE JSSC*, vol. 50, no. 11, pp. 2758–2772, Nov. 2015.

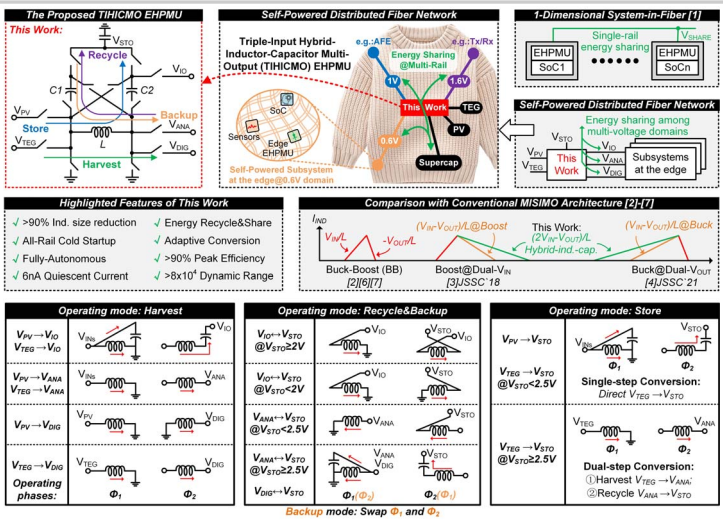

Figure 8.5.1: The proposed TIHICMO EHPMU for self-powered distributed fiber network with multi-voltage domain energy sharing (top); comparison to the traditional MISIMO architecture (middle); the phases of the four operating modes that the proposed EHPMU supports (bottom).

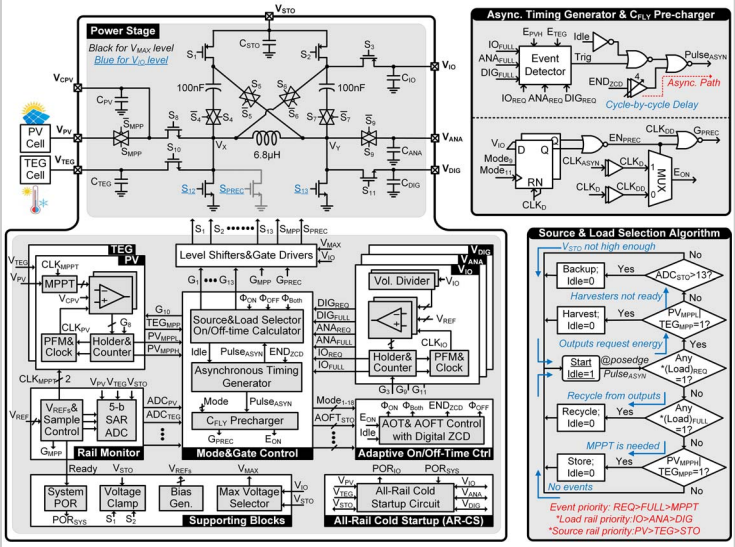

Figure 8.5.2: System block diagram of the proposed TIHICMO EHPMU (left); the schematic of asynchronous timing generator and C_{FLY} pre-charger (top-right); flow chart of the source and load selection algorithm (bottom-right).

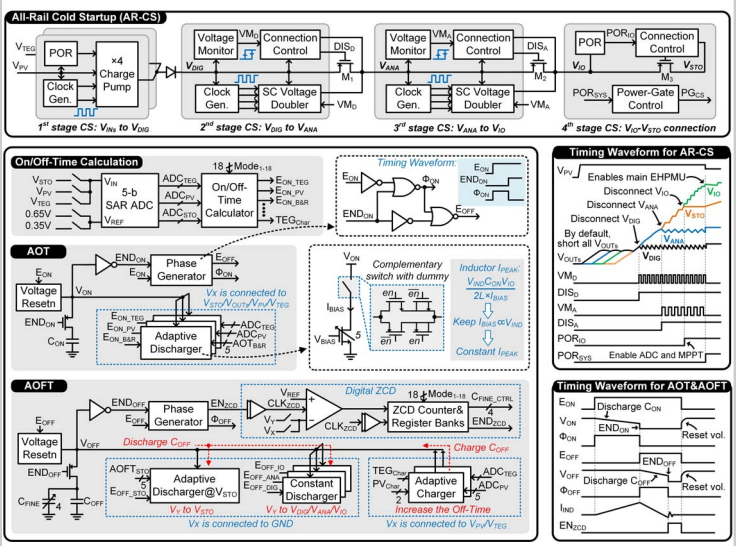

Figure 8.5.3: Schematic of the proposed AR-CS (top), on/off-time calculation, adaptive-on-time (AOT) control, and adaptive-off-time (AOFT) control (bottom-left); the timing waveform for the AR-CS, AOT and AOFT (right).

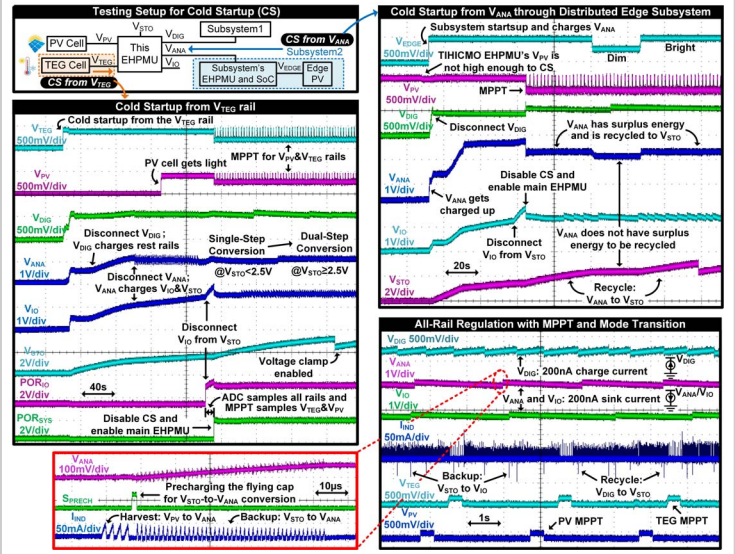

Figure 8.5.4: Testing setups for the CS waveforms (top); measured waveform for cold startup from V_{TEG} (left) and V_{ANA} rail (middle); measured waveform for rail regulation and mode transition with zoomed-in details (bottom).

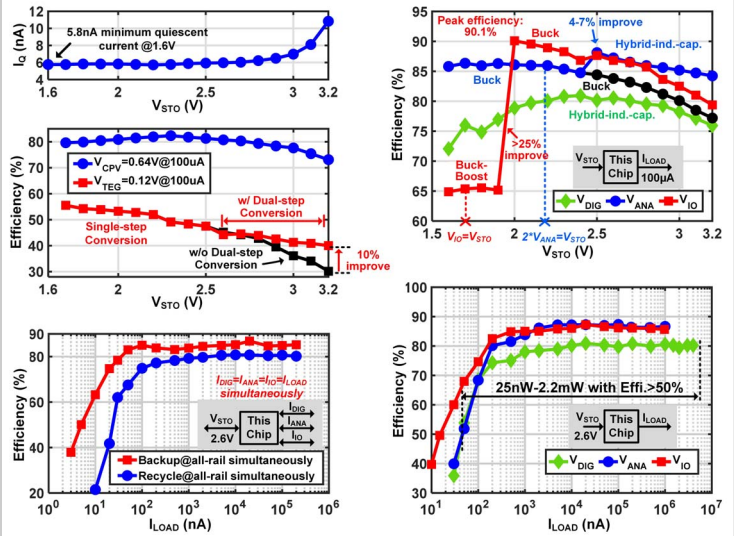

Figure 8.5.5: Measured EHPMU quiescent current and harvesting efficiency vs. V_{STO} (top-left); measured efficiency for recycle and backup mode vs. I_{LOAD} (bottom-left); measured efficiency for backup mode vs. V_{STO} and I_{LOAD} (right).

	[7] JSSC'15	[3] JSSC'18	[4] JSSC'21	[5] JSSC'19	[6] ISSCC'18	[2] ISSCC'22	This Work
Technology	180nm	180nm	180nm	180nm	28nm	65nm	**65nm**
No. of Inputs	1 + battery	2 + supercap	3 + battery	3 + supercap	3 + battery	3 + supercap	**2 + supercap**
No. of Outputs	2 + battery	2 + supercap	3 + battery	1 + supercap	3 + battery	4 + supercap	**3 + supercap**
Input Sources	PV	PV/TEG	PV/TEG/BFC	PV/TEG	PV/TEG/BFC	PV/TEG/PEH	**PV/TEG**
EHPMU Architecture	1-stage, 1-inductor	1-stage, 1-inductor	1-stage, 1-inductor	1-stage, 1-inductor	1-stage, 1-inductor	1-stage, 1-inductor	**1-stage, 1-inductor, 2-flying capacitors**
Conversion Mode	Buck-Boost	Buck-Boost /Buck	Buck-Boost /Buck/Boost	Buck-Boost	Buck-Boost	Buck-Boost	**Buck-Boost/ Buck/Boost/ Hybrid-ind.-cap.**
Inductor Current Control	Fixed On-Time	AOT(APIC)	AOT(APIC)	Fixed On-Time	AOT(Hysteresis)	AOT(ADC)	**AOT (APIC)**
L & C_{FLY}	10μH	4.7μH	4.7μH	4.7μH	10μH	22μH	**6.8μH & 100nF×2**
L Size (mm) & DCR (Ω)	5.8×5.2×4.5	N/R	N/R	N/R	N/R	6×6×3.5, 0.15	**3×3×1.3, 0.2**
C_{LOAD}	10μF	1μF	2.2μF	10μF	1μF	4.7μF	**10μF & 4.7μF**
V_{OUTS} (V) & V_{STO} (V)	1/1.8 & 2.5	0.5/1.2 & 1.2	1/1.3/1.6 & 2.4	1.2 & (-0.6)	0.4 - 1.4 & 1.8	0.6/0.6/1.2/3.3 & 3.3	**0.6/1/1.6 & 3.2**
Energy Recycling/Sharing	No	No	No	No	No	No	**Yes (Multi-Rail)**
Quiescent Power or Current	400nW	>10μW*	>300nW	>500nW	262nA@1V	12nA@2.8V (PV+TEG only)	**5.8nA@1.6V**
Output Power with Efficiency>50%	1μW~10mW	20μW~4mW (133×)	1μW~2.4mW (2,400×)	6μW~10mW* (833×)	1μW~60mW (60,000×)	40nW~3.3mW* (82,500×)	**25nW~2.2mW (88,000×)**
Efficiency @ 1μA I_{LOAD}	68%	N/A	69.0%	<50%	<76%	80%	**85%**
Peak Efficiency	83%	84.4%	90.2%	82.1%	89%	81.5%	**90.1%**
Cold Startup	No	No	No	Yes (PV only)	No	Yes (Input Rails only)	**Yes (All Input/Ouput Rails)**
Area (mm^2)	4.62	2.9	2.58	1.23	0.5 (active area)	3.11	**2.8**

N/R=Not Reported; N/A= Not Applicable
*Estimated from the figures in the paper

Figure 8.5.6: Comparison of the proposed EHPMU with state-of-the-art MISIMO EHPMUs.

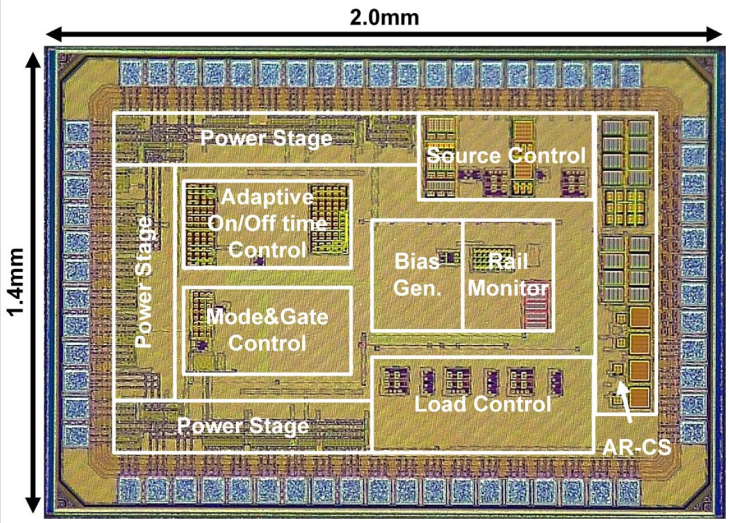

Figure 8.5.7: Die micrograph of the proposed TIHICMO EHPMU.

979-8-3503-0620-0/24/$31.00 ©2024 IEEE